REPORT DOCUMENTATION PAGE

Form Approved
OMB No. 0704-0188

Public reporting burden for this collection of information is estimated to average 1 hour per response, including the time for reviewing instructions, searching existing data sources, gathering and maintaining the data needed, and completing and reviewing this collection of information. Send comments regarding this burden estimate or any other aspect of this collection of information, including suggestions for reducing this burden to Department of Defense, Washington Headquarters Services, Directorate for Information Operations and Reports (0704-0188), 1215 Jefferson Davis Highway, Suite 1204, Arlington, VA 22202-4302. Respondents should be aware that notwithstanding any other provision of law, no person shall be subject to any penalty for failing to comply with a collection of information if it does not display a currently valid OMB control number. **PLEASE DO NOT RETURN YOUR FORM TO THE ABOVE ADDRESS.**

1. REPORT DATE (DD-MM-YYYY)	2. REPORT TYPE	3. DATES COVERED (From - To)
10-12-2010	Final Technical Report	December 2006 – May 2010

4. TITLE AND SUBTITLE
Atmospheric polarization imaging with variable aerosols

and clouds

5a. CONTRACT NUMBER

5b. GRANT NUMBER
FA9550-07-1-0011

5c. PROGRAM ELEMENT NUMBER

6. AUTHOR(S)

Dr. Joseph A. Shaw

5d. PROJECT NUMBER

5e. TASK NUMBER

5f. WORK UNIT NUMBER

7. PERFORMING ORGANIZATION NAME(S) AND ADDRESS(ES)
Montana State University
Office of Sponsored Programs
307 Montana Hall
Bozeman, MT 59717-0001

8. PERFORMING ORGANIZATION REPORT NUMBER

9. SPONSORING / MONITORING AGENCY NAME(S) AND ADDRESS(ES)
Air Force Office of
Scientific Research

875 N. Randolph St., Rm. 3112
Arlington, VA 22203

10. SPONSOR/MONITOR'S ACRONYM(S)

11. SPONSOR/MONITOR'S REPORT NUMBER(S)
AFRL-OSR-VA-TR-2012-0711

12. DISTRIBUTION / AVAILABILITY STATEMENT

Unlimited -A

13. SUPPLEMENTARY NOTES

14. ABSTRACT
An all-sky polarization spectral imager developed under prior support was deployed along with an atmospheric lidar, a sun-tracking multi-channel solar radiometer, an infrared cloud imager, and a variety of ground-based aerosol sensors to study the effect of variable clouds and aerosols on skylight polarization in the 450 – 780 nm spectral region. Near the end the performance period the imaging polarization imager was re-engineered to operate in an autonomous manner outdoors in a weather-proof housing to allow long-term collection of data in a wide range of conditions. This study has shown that clouds always significantly alter the degree of polarization of skylight (either below the cloud or in a cloud-free portion of the sky), but that they often do not alter the angle of polarization beneath the clouds. Under certain illumination conditions, the angle of polarization beneath a cloud is rotated by 90-degrees relative to the clear-sky polarization. A relationship also was developed for an initial model of how increasing surface albedo reduces the overhead skylight polarization.

15. SUBJECT TERMS
Remote sensing, atmospheric propagation,

16. SECURITY CLASSIFICATION OF:			17. LIMITATION OF ABSTRACT	18. NUMBER OF PAGES	19a. NAME OF RESPONSIBLE PERSON
a. REPORT	b. ABSTRACT	c. THIS PAGE			19b. TELEPHONE NUMBER (include area code)

Standard Form 298 (Rev. 8-98)
Prescribed by ANSI Std. Z39.18

Final Report: Atmospheric Polarization Imaging with Variable Aerosols and Clouds

Dr. Joseph A. Shaw (jshaw@montana.edu), Montana State University – Bozeman

Executive Summary

Effective prediction and exploitation of polarization signatures in optical remote sensing requires improved understanding of the underlying physical mechanisms and phenomenology. To this end we have developed and deployed an all-sky polarization imager, along with a wide range of atmospheric sensors, to study the influence of aerosols and clouds on skylight polarization in the visible and near-infrared spectral bands. We developed the all-sky polarization imager with prior AFOSR support, and this report focuses on its deployment and on some of its primary results. Key results include the following:

- The clear atmosphere exhibits a pattern of skylight polarization that can be predicted from Rayleigh scattering theory, with a band of maximum degree of polarization located 90° from the sun, but in the real atmosphere this polarization maximum is significantly lower than the theoretical 100% predicted by single Rayleigh scattering (reasons include multiple Rayleigh scattering by non-point scatterers, an always-present small amount of aerosols that are larger than Rayleigh particles, and a non-zero surface reflectance);
- Increased aerosol concentration reduces the degree of polarization at all spectral bands;
- Clouds reduce the degree of polarization at all spectral bands, even in a cloud-free portion of the sky away from an isolated cloud;
- Clouds often do not alter the angle of polarization for skylight below the cloud;
- Under certain illumination conditions (particularly when the cloud is located in a region of weak skylight polarization so that the cloud scattering dominates), the angle of polarization observed beneath a cloud is oriented 90° relative to the clear-sky value;
- Polarization fluctuations have been observed in our data up to several hours prior to the appearance of a visible cloud in a previously clear sky, suggesting that the polarization may be a highly sensitive indicator of aerosol growth that leads to a cloud;
- Measurements made at the Mauna Loa Observatory (a mountaintop observatory in Hawaii) confirmed previous studies by Coulson and extended them to partly cloudy conditions;
- The Mauna Loa measurements led to an initial relationship between surface reflectance and the resulting decreased clear-sky degree of polarization.

This effort (Dec. 2006 – May 2010) involved four researchers:
1. Dr. Joseph A. Shaw – Professor and principal Investigator
2. Dr. Nathan J. Pust – postdoctoral associate
3. Mr. Andrew Dahlberg – graduate student working primarily on Mauna Loa polarization
4. Mr. Paul Nugent – graduate student working primarily on cloud imaging and later Research Engineer (supported primarily with NASA funding, but partly supported by AFOSR polarization funds)

Two graduate students successfully defended Master of Science theses based partly or fully on work supported by this grant:

1. Mr. Andrew Dahlberg – *All-sky polarization imager deployment at Mauna Loa Observatory, Hawaii* – M.S. Thesis, May 2010 (http://etd.lib.montana.edu/etd/view/item.php?id=1048).
2. Mr. Paul Nugent – *Wide-angle infrared cloud imaging for cloud cover statistics*, M.S. Thesis, May 2008 (http://etd.lib.montana.edu/etd/view/item.php?id=642).

The following **journal papers** have been generated with full or partial support from this project:

1. N. J. Pust and J. A. Shaw, "Digital all-sky polarization imaging of partly cloudy skies," *Appl. Opt.* **47**(34), H190-H198 (doi:10.1364/AO.47.00H190), Dec. 2008.
2. P. W. Nugent, J. A. Shaw, and S. Piazzolla, "Infrared cloud imaging in support of Earth-space optical communication," *Opt. Express* **17**(10), 7862-7872, 11 May 2009.
3. P. W. Nugent, J. A. Shaw, N. J. Pust, and S. Piazzolla, "Correcting calibrated infrared sky imagery for the effect of an infrared window," *J. Atmos. Oceanic Technol.* **26**(11), 2403-2412, doi:10.1175/2009JTECHA1288.1, Nov. 2009.
4. K. S. Repasky, J. A. Reagan, A. R. Nehrir, D. S. Hoffman, M. J. Thomas, J. L. Carlsten, J. A. Shaw, and G. E. Shaw, "Observational studies of atmospheric aerosols over Bozeman, Montana using a two color lidar, a water vapor DIAL, a solar radiometer, and a ground based nephelometer over a twenty four hour period," *J. Atmos. Ocean Technol.* **27**, doi:10.1175/2010JTECHA1463.1 (2010).
5. N. J. Pust and J. A. Shaw, "Comparison of skylight polarization measurements and MODTRAN-P calculations," *J. Applied Remote Sensing* (submitted spring 2010).

The following **conference papers** were published with full or partial support from this project:

1. P. W. Nugent, J. A. Shaw, and S. Piazzolla, "Wide-angle infrared cloud imaging for measuring cloud statistics in support of Earth-Space optical communication," *Proc. SPIE* **6709** (*Free-Space Laser Communications VII,* San Diego, CA), 67090F-1-9, Aug. 2007.
2. J. A. Shaw and N. J. Pust, "All-sky polarization imaging," *Proc. SPIE* **6682** (*Polarization Scence and Remote Sensing III,* San Diego, CA), 668204-1-6 Aug. 2007.
3. J. A. Shaw, "A survey of infrared polarization in the outdoors," Invited paper, *Proc. SPIE* **6660** (*Infrared Detectors and Focal Plane Arrays*, San Diego, CA), 666006-1-10, Aug. 2007.
4. N. J. Pust, J. A. Shaw, A. Dahlberg, "All-sky imaging polarimetry," Optical Technology Center Annual Meeting, Montana State University, Bozeman, MT, 20 Sep. 2007.
5. J. A. Shaw (by E. R. Westwater), "Wide-angle infrared cloud imaging," DoE Atmospheric Radiation Measurement (ARM) program, Cloud Properties Working Group meeting, Annapolis, MD, 13 Nov. 2007.
6. N. J. Pust, J. A. Shaw, and A. R. Dahlberg, "Visible-NIR imaging polarimetry of metal surfaces viewed under a variable atmosphere," Proc. SPIE **6972** (*Polarization: Measurement, Analysis, and Remote Sensing VIII,* Orlando, FL), 18-19 Mar. 2008.
7. P. W. Nugent and J. A. Shaw, "Large-area blackbody emissivity variation with observation angle," Proc. SPIE **7300** (*Infrared Imaging Systems: Design, Analysis, Modeling, and Testing XX*), Orlando, FL, 14 April 2009 (doi:10.1117/12.819223).

8. N. J. Pust and J. A. Shaw, "How good is a single-scattering model of visible-NIR atmospheric skylight polarization?" Proc. SPIE **7461** (*Polarization Science and Remote Sensing IV*), 74610B, 3 Aug. 2009 (doi:10.1117/12.828343).
9. N. J. Pust, J. A. Shaw, A. R. Dahlberg, "Concurrent polarimetric measurements of painted metal and illuminating skylight compared with a microfacet model," Proc. SPIE **7461** (*Polarization Science and Remote Sensing IV)*, 74610X, 3 Aug. 2009 (doi:10.1117/12.826546).
10. A. R. Dahlberg, N. J. Pust, J. A. Shaw, "All-sky imaging polarimeter measurements of visible and NIR skylight at Mauna Loa, Hawaii," Proc. SPIE **7461** (*Polarization Science and Remote Sensing IV*), 746107, 3 Aug. 2009 (doi:10.1117/12.826537).
11. J. A. Shaw, N. J. Pust, B. Staal, J. Johnson, A. Dahlberg, "Continuous outdoor operation of an all-sky polarization imager," Proc. SPIE **7672** (*Polarization: Measurement, Analysis, and Remote Sensing IX*), 76720A-1-7, 7 April 2010 (doi:10.1117/12.851374).

The following **conference presentations** were given (without published paper) with partial or full support from this project:

1. J. A. Shaw and N. J. Pust, "All-sky polarization imaging," 9th International Meeting on Light and Color in Nature, Montana State University, Bozeman, MT, 25-29 June, 2007.
2. P. W. Nugent, J. A. Shaw, and S. Piazzolla, "Wide-angle infrared imaging for measuring clouds for Earth-space optical communications," URSI National Radio Science Meeting, Boulder, CO, 5-8 Jan. 2008.
3. A. Dahlberg, N. J. Pust, and J. A. Shaw, "All-sky imaging polarimeter deployment at Mauna Loa, Hawaii," Optical Technology Center (OpTeC) annual meeting, Montana State University, Bozeman, MT, 27 Aug. 2008.
4. P. W. Nugent, J. A. Shaw, and S. Piazzolla, "Infrared cloud imaging in support of Earth-space optical communication," Optical Technology Center (OpTeC) annual meeting, Montana State University, Bozeman, MT, 27 Aug. 2008.
5. J. Johnson, P. W. Nugent, K. Simpson, B. Staal, and J. A. Shaw, "Microcontroller and mechanical design for the new-generation infrared cloud imager," Optical Technology Center (OpTeC) annual meeting, Montana State University, Bozeman, MT, 27 Aug. 2008.
6. J. A. Shaw, N. J. Pust, and A. Dahlberg, "All-sky polarization imaging in variably cloudy skies," National Radio Science Meeting (URSI), Boulder, CO, 6 January 2009.
7. A. R. Dahlberg, N. J. Pust, J. A. Shaw, "Methods for displaying all-sky polarization imager data," poster-only presentation at SPIE *Polarization Science and Remote Sensing IV,* San Diego, CA, 3 Aug. 2009.
8. P. W. Nugent and J. A. Shaw, "Radiometric calibration of low-cost, non-thermally stabilized infrared imagers," Optical Technology Center (OpTeC) annual meeting, Montana State University, Bozeman, MT, 20 Aug. 2009.
9. A. R. Dahlberg, N. J. Pust, J. A. Shaw, "methods for displaying all-sky polarization imager data," Optical Technology Center (OpTeC) annual meeting, Montana State University, Bozeman, MT, 20 Aug. 2009.
10. J. A. Shaw, "Atmospheric effects on polarization," Workshop on polarimetry in space-situational awareness, Air Force Research Laboratory, Albuquerque, NM, 9 Feb. 2010.

11. A. Dahlberg, N. J. Pust, and J. A. Shaw, "All-sky imaging of visible-wavelength atmospheric polarization at Mauna Loa, Hawaii," Proc. International Geoscience and Rem. Sens. Symposium (ISBN 978-1-4244-9566-5), 1683-1686, 25 July 2010.
12. K. S. Repasky, A. R. Nehrir, D. S. Hoffman, M. J. Thomas, J. L. Carlsten, J. A. Shaw, "Observational studies of atmospheric aerosols in the lower troposphere using multiple sensors," Proceedings of the International Geoscience and Remote Sensing Symposium (ISBN 978-1-4244-9566-5), 2583-2586, 25 July 2010.
13. A. R. Dahlberg, N. J. Pust, J. A. Shaw, "All-sky polarization imaging at Mauna Loa, Hawaii," Optical Technology Center (OpTeC) annual meeting, Montana State University, Bozeman, MT, 26 Aug. 2010.
14. N. J. Pust, A. R. Dahlberg, J. A. Shaw, "Full-sky radiance models," Optical Technology Center annual meeting, Montana State University, Bozeman, MT, 26 Aug. 2010.
15. M. Thomas, J. A. Shaw, N. J. Pust, G. E. Shaw, K. S. Repasky, J. A. Reagan, "In-situ and solar radiometer measurements of aerosols over MSU," Optical Technology Center (OpTeC) annual meeting, Montana State University, Bozeman, MT, 26 Aug. 2010.
16. J. A. Shaw, N. J. Pust, A. R. Dahlberg, "All-sky polarization imaging," Invited talk at MISR User's Workshop, California Institute of Technology, Pasadena, CA, 9-10 Dec. 2010.
17. M. J. Thomas, T. L. Lathem, J. A. Shaw, G. E. Shaw, A. Nenes, N. J. Pust, K. S. Repasky, "Aerosols in clean and smoky air at Bozeman, Montana," American Geophysical Union (AGU) Fall Meeting, San Francisco, CA, 13-17 Dec. 2010.
18. N. J. Pust, J. A. Shaw, A. R. Dahlberg, "Comparison of observed full-sky polarization to radiative transfer model using AERONET retrieval inputs," American Geophysical Union (AGU) Fall Meeting, San Francisco, CA, 13-17 Dec. 2010.

Introduction

Polarization-sensitive imaging provides the possibility of enhancing detection of man-made objects in low-contrast scenes and enhancing the accuracy of remotely sensed atmospheric properties, such as optical properties of aerosols that obscure a battlefield or modulate the earth's climate. However, effective prediction and exploitation of polarization signatures requires thorough understanding of the physics giving rise to the object and background signatures.

The atmospheric variables that most strongly influence polarization signatures at visible and near-infrared wavelengths are aerosol and cloud distributions and optical properties. Humidity also plays a role, but primarily through growth of aerosols and clouds. At these wavelengths, a clear sky has a distinct pattern of partially polarized light that peaks in a band stretching across the sky 90° from the Sun. The theory of a single Rayleigh scattering event predicts that the degree of polarization (DoP) in this band will be 100%, but in reality multiple scattering reduces the maximum value significantly, often well below 70%. Aerosols and cloud particles, whose sizes are comparable to or larger than the optical wavelength, alter the pure Rayleigh background through scattering processes that do not follow the simple Rayleigh law. Consequently, predicting the observed degree of polarization in skylight in nearly all realistic conditions requires careful consideration of clouds and aerosols.

In response to this need for atmospheric polarization prediction capability, the Air Force Research Laboratory (AFRL) is developing a polarized Modtran (Mod-P) radiative transfer code.

However, in any one model run only a single atmospheric path can be characterized. That path can be modeled as clear or cloudy, but not partly cloudy. Similarly, a spatially variable distribution of aerosols cannot be simulated without multiple model runs. Related to this is the inability to model spatially variable surface albedo (i.e., ground reflectance). Therefore, there is a need to understand more about how variable aerosols, clouds, and surface albedo influence atmospheric polarization distributions. There is a related need to understand more about how the resulting sky polarization patterns (and other meteorological variables) influence polarization signatures of man-made objects observed outdoors.

To illustrate these questions further, consider a situation where the sky is cloudy in one area and clear in another. Would the MOD-P code predict the proper polarization state from the clear patch, even though it cannot simultaneously include the influence of the cloudy patch? Would it predict the proper polarization state from the cloudy patch, even though it cannot simultaneously include the influence of the clear patch? Would these values be significantly different from those that would be found under totally cloudy or totally clear conditions? Our research has used an all-sky Atmospheric Polarization Imager (API) instrument to show that the polarization state of light observed at one point in the sky can vary significantly as the clouds and aerosols change in another part of the sky. For example, the maximum degree of observed polarization in a clear portion of the sky is often notably lower when clouds exist in other parts of the sky (Pust and Shaw 2006, 2008). We have also observed significant variation of skylight polarization with aerosol content and surface albedo. For example, the maximum degree of polarization in a visibly clear sky at a wavelength of 450 nm was observed to vary from 80% to less than 50% as haze built up from forest fire smoke (Pust and Shaw 2006). Furthermore, variations in the underlying surface albedo appear to explain a morning-to-afternoon asymmetry in the observed polarization pattern in the sky above the Mauna Loa Observatory on the island of Hawaii (Dahlberg et al. 2009).

The Atmospheric Polarization Imager (API) System

The API instrument that we designed, built, calibrated, and operated extensively expands the capabilities of previous all-sky polarization imagers to enable the first quantitative studies of sky polarization in partly cloudy skies. For example, it provides real-time digital data and removes the uncertainty of film processing inherent in systems described by North and Duggin (1997) and Horvath et al. (2002). Our use of electronically tunable liquid crystal variable retarders (LCVRs) allows the API to achieve much faster Stokes-image acquisition than instruments that rely on rotating polarization elements (Cronin et al. 2006; Voss and Liu 1997; Liu and Voss 1997), enabling operation in changing cloud conditions without polarization artifacts. The API instrument records a Stokes vector at each pixel of a 1-Mpixel image of the full sky dome in approximately 0.3-1.3 s, depending on the required exposure time (Pust and Shaw 2006). The four elements of the Stokes vector, or Stokes parameters, completely describe the polarization state of the light detected at each pixel. These parameters are used to calculate the degree of polarization (DoP), which expresses the percentage of the incident light that is polarized (or degree of linear polarization, DoLP, with only linear polarization), and the angle of polarization (AoP), which expresses the orientation of the polarized light.

The API system achieves rapid polarimetric tuning through the use of LCVRs and a fixed linear polarizer, but relies on a rotating filter wheel for the slower spectral tuning that can be accepted

in these studies. The system can be used with a fisheye front-end optics module for all-sky imaging, or a telephoto module for remote target polarization signature imaging. Figure 1 is an optical layout for the system with fisheye optics. The front-end optical module at the left is followed by two field lenses that direct wide-angle light into the polarimeter to the right. The front-end optics assembly screws onto the LCVR-based polarimeter, which feeds the light through a filter wheel fitted with 10-nm-wide filters (originally at 450, 490, 530, 630, and 700 nm, but changed in 2010 to 450, 490, 530, 670 and 780 nm to avoid weak atmospheric absorption features present in the prior channels). A micro-Nikkor reimaging lens matches the image size to the CCD detector array. The LCVRs are electronically tuned to four optimal retardance states (Tyo 2000, 2002; Sabatke 2000), and a system matrix found from images at these states allows calculation of a Stokes vector at each pixel (Pust and Shaw 2006). The uncertainty in the degree of polarization (DOP) is within 2% for any linear polarization state, but is often much better (see Table 1).

Figure 1. Diagram of the Atmospheric Polarization Imager (API) system with fisheye front-end optics for imaging the full sky dome. The liquid crystals allow rapid polarimetric imaging with changing clouds and aerosols (a telephoto front-end optics module can be used to achieve imaging in a narrower field of view when necessary).

Aerosol and Cloud Polarization Effects

Episodic deployments at the Montana State University campus have led to the identification of a number of interesting things about skylight polarization during partly cloudy conditions that the API is uniquely capable of studying. An example of this, which was discussed with less certainty in our previous final report (2007), is shown in Fig. 2. This figure shows the measured DoLP for the full sky dome, which was entirely clear for the left-hand image and clear except for one distinct cloud for the right-hand image. The only significant difference between these images, which were taken at the same solar elevation angle three days apart, was the small cloud. The arc of high polarization at angles 90˚ from the Sun is clearly visible in both images, but the maximum DoLP is notably lower in the right-hand image (~58%) relative to the left-hand image (~66%). In other words, the polarization in the clear portion of a mostly clear sky is significantly different from that in a truly clear sky. This appears to arise because of multiple scattering from an invisible veil of aerosols that extends well beyond the cloud edges (Pust and Shaw 2008).
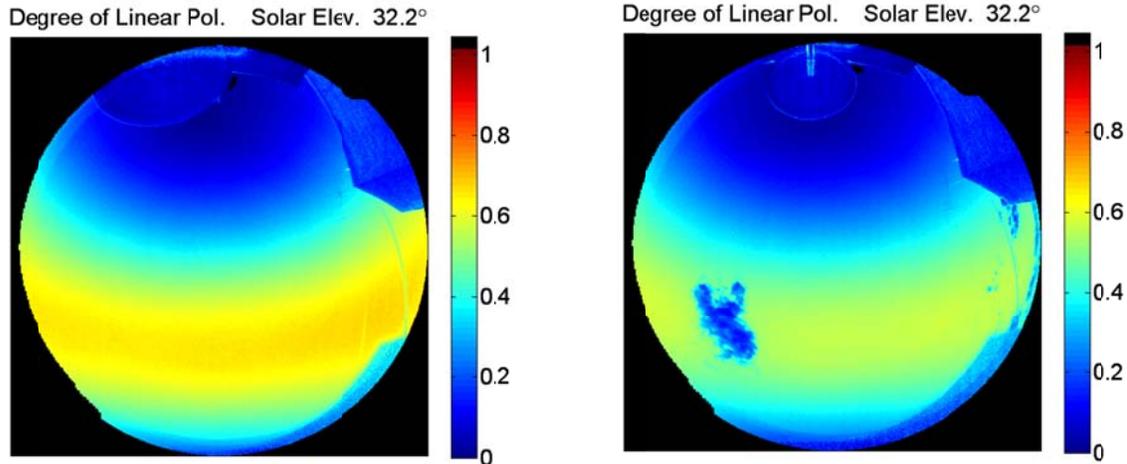
Fig. 2. DoLP sky images at 450 nm for (left) a clear sky (26 June 2006, 23:55 UTC) and (right) a mostly clear sky containing small isolated clouds (23 June 2006, 2355 UTC).

The reduction of DoLP in an apparently clear portion of a partly cloudy sky (Fig. 2) appears to be caused by elevated aerosol content well beyond a cloud edge. In other words, clouds do not have sharp edges. How rapidly the aerosols decay away from a cloud "edge" is a very active research question at the moment (Koren et al. 2007, 2008; Charlson et al. 2007) and it turns out the API instrument has unique capabilities for studying this effect. The red and green curves in Fig. 3 show the maximum sky DoLP following a relatively repeatable curve throughout days that remain cloud free. However, the blue curve in Fig. 3 is for a day when clear-sky conditions gave way to a few small isolated clouds late in the afternoon (same day as Fig. 2). On this day, the max DoLP curve began fluctuating significantly from the expected clear-sky curve nearly three (3) hours before any clouds were visible by eye (gray shading).
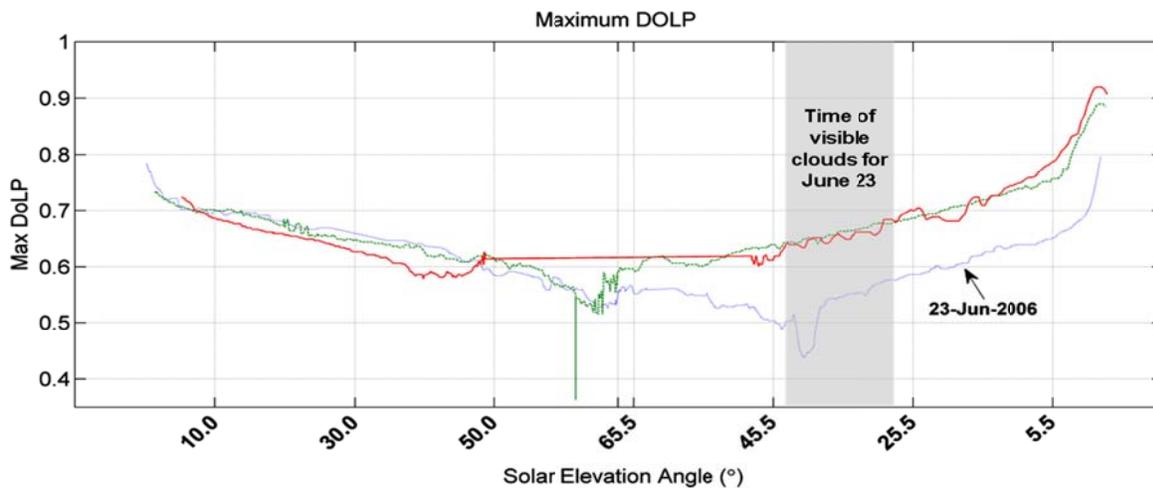

Fig. 3. Maximum DoLP at 700 nm for 23 June, 26 June, and 11 September, 2006. On 23 June the maximum DoLP curve indicates cloud precursors several hours before clouds were visible. The sky was completely cloud free on 26 June and 11 Sept., but on 23 June it was cloud free except in the gray-shaded time when a few small, localized clouds were visible (see Fig. 4).

Our work also provided an explanation of the conditions under which the angle of polarization beneath a cloud (AoP) can deviate from the clear-sky pattern (Pust and Shaw 2008). The DoP pattern can change very significantly in the presence of clouds, but previous authors had claimed that the AoP continues unaffected beneath a cloud (Pomozi et al. 2001). Although we do see many images where the AoP pattern continues unaffected below a cloud, Fig. 4 is an example where the AoP pattern changes significantly from the clear-sky pattern (Pust & Shaw 2008). In this image, clouds primarily in the upper-right portion of the image exhibit an AoP that is rotated by 90˚ from the clear-sky AoP at the same image point. This is an extremely significant shift that could make an enormous difference in the influence that this atmosphere would have on the polarization signature observed from a ground-based or airborne object. A model that assumes the AoP always continues unchanged below a cloud would be in gross error in this case.
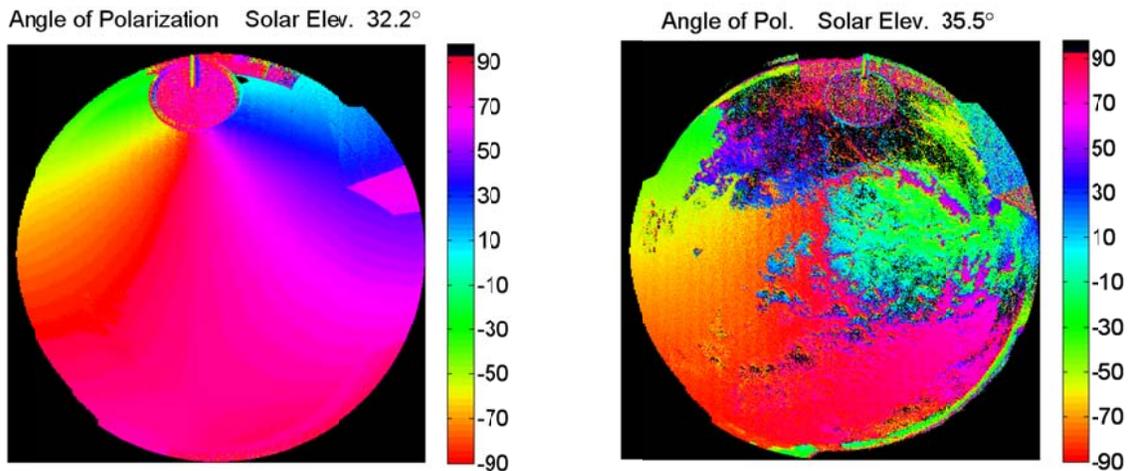

Fig. 4. Angle of Polarization (AoP) images for (left) a clear sky and (right) a partly cloudy sky. Whereas the clear-sky AoP pattern often continues unchanged below a cloud, the case shown on the right-hand side exhibits a 90˚ rotation of the AoP relative to the clear-sky pattern.

As is explained in Pust and Shaw (2008), the 90˚ rotation of the AoP in the right-hand image of Fig. 4 arises when either (1) the direct sunlight is obscured by clouds, or (2) clouds are located in sky regions away from the band of high clear-sky DoLP. Depending on the size distribution and density of cloud particles, the light scattered by the cloud can be polarized either parallel or perpendicular to the scattering plane (defined by the source, scattering object, and observer), whereas Rayleigh scattered light from the clear atmosphere is always partially polarized perpendicular to the scattering plane. The AoP beneath the cloud can be oriented 90˚ from the clear-sky pattern when a liquid cloud with just the right size of particles is situated such that the cloud-scattered light dominates the Rayleigh scattered light from the molecular column below the cloud (Pust and Shaw 2008).

Atmospheric Effects on Polarization Signatures of Metal Plates

The API instrument was operated with a telephoto front-end optics module for measuring the polarization signature of metal plates in a narrower field of view. Figure 5 shows a photograph of

the instrument used in this configuration to measure the polarization signatures of smooth and rough, tan and black, metal plates under variable cloud conditions (Pust et al. 2009b, 2008). An example of these measurements is shown in Fig. 6 as a plot of the smooth tan plate DoLP at 450-nm wavelength versus solar elevation angle (i.e, time) for a full day. Data are shown for two sequential days with nearly symmetric sky conditions: 27 September was overcast in the morning and clear in the afternoon, while 28 September was clear in the morning and partly cloudy in the afternoon.

Fig. 5. Photograph of the API fitted with the telephoto front optics module to measure the polarization signature of smooth and rough metal plates under variable cloud conditions.
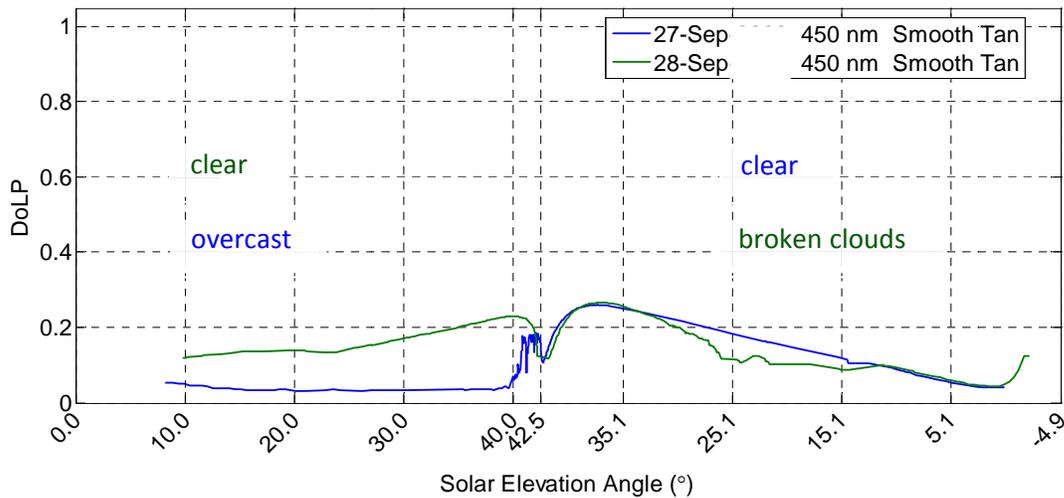

Fig. 6. DoLP measured from the smooth tan plate during two sequential days with symmetric cloud conditions (cloudy morning + clear afternoon, followed by clear morning + cloudy afternoon). The clouds greatly suppress the observed polarization, but this effect depends strongly on wavelength, paint color, and plate roughness (not shown here).

The polarization observed from the metal plates changes significantly between cloudy and clear conditions, illustrating the importance of properly characterizing clouds for predicting and interpreting polarization signatures. The cloud effects vary strongly with wavelength, with some variation apparently a consequence of the paint's reflectance spectrum. Also, the observed polarization is significantly higher for the black plates than tan ones and, for any given color, is higher for smooth plates than for rough plates.

Field Deployment of the API at the Mauna Loa Observatory – May & June 2008

To obtain measurements in a clean atmosphere that is as close to a pure Rayleigh scattering situation as possible without leaving Earth's atmosphere, we conducted a major field experiment with our API instrument at the Mauna Loa Observatory (MLO) on the island of Hawaii during May and June 2008. This facility is also located relatively near the Air Force Maui Optical Station on the next island over (Maui), and this has led to ongoing talks with Air Force personnel regarding the possibility of deploying our system at Maui to characterize this facility as well.

Figure 7 is a photograph of the API system deployed in the all-sky imaging mode with fisheye front-end optics at the MLO. The cables connect the optical system with a computer and electronics rack located in a nearby shelter. The object shown at the left is a telescoping rod holding a disk to prevent direct imaging of the Sun (i.e., a "Sun occulter"), which could damage the CCD and obliterate the polarization data.

Figure 7. The API system in fisheye mode, deployed at the Mauna Loa Observatory (Hawaii) in May 2008.

The careful and frequent attention required to manually move a Sun occulter throughout the day is no longer required since we developed an automated sun occulter after returning from the Mauna Loa experiment. The new occulter tracks the sun through the sky with microprocessor-controlled azimuth and elevation motors, as shown in Fig. 8(left), and allows the instrument to operate without an operator standing by to move the occulter. Figure 8(right) is a photograph of

the new occulter (Shaw et al. 2010) on a new environmentally sealed enclosure that is being refined and tested in our ongoing research effort.
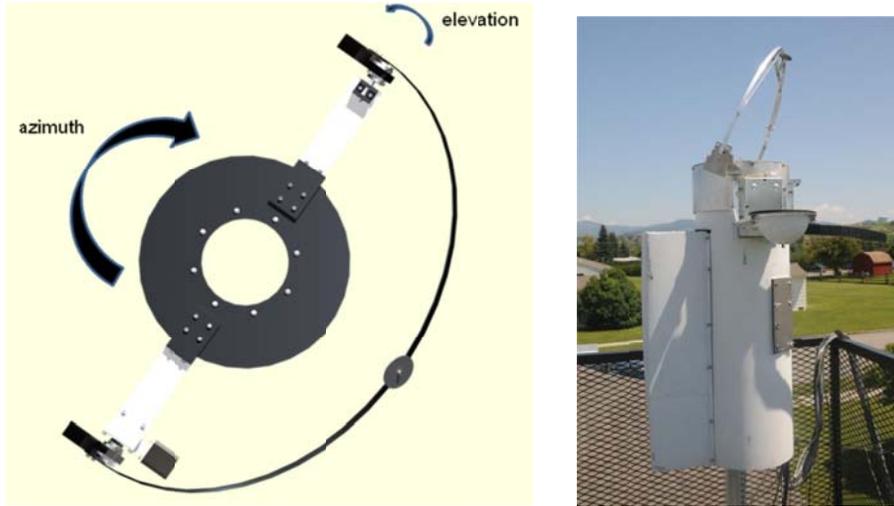

Fig. 8. (left) Mechanical drawing of the new automated sun occulter assembly; (right) photograph of the API system with the automated occulter in a newly designed weather-hardened enclosure.

During the MLO deployment, all-sky polarization images such as those in Fig. 9 (for 700 nm) were produced on 1-2 minute intervals for each of the five wavelengths. In this early morning image with clear sky overhead, we see the characteristic maximum Degree of Linear Polarization (DoLP) arc stretch across the sky, with a flare at the edges caused by the fisheye lens. The DoLP in this experiment reached approximately 89%, the highest we have measured anywhere. The sun, still not in the FOV of the imager, moves across the sky from left to right, rotating this arc throughout the day. Figure 9b shows the mapping of the effective scattering angle α to the fisheye reference plane. Note how the black contour at 90° correlates well with the maximum DoLP band in the left image.
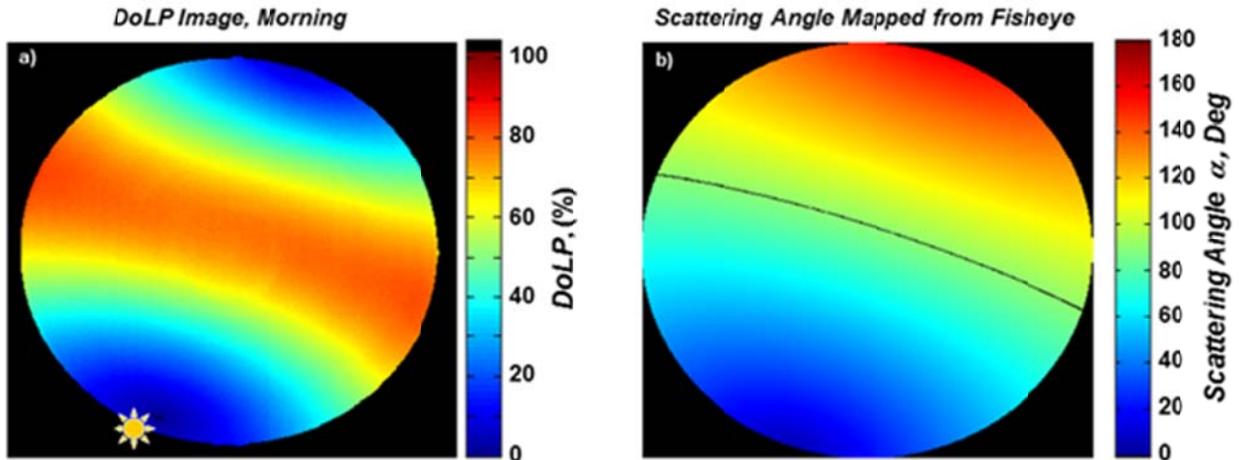

Figure 9: (a) DoLP image of a clear morning with the sun to the east. (b) The scattering angle (with respect to the sun) mapped to the fisheye lens image plane.

The MLO experiment provided measurements of the highest DoLP values we have observed anywhere as of this writing and also allowed the validation of previous measurements made with a scanning filter-wheel instrument (Coulson 1988). The API measurements do not include the shortest wavelengths that Coulson used, but generally fall within his range of results obtained under similar conditions, as indicated in Fig. 10, which shows a plot of the maximum DoLP vs. wavelength with the curve fits to Coulson's data shown as partial font in the background.
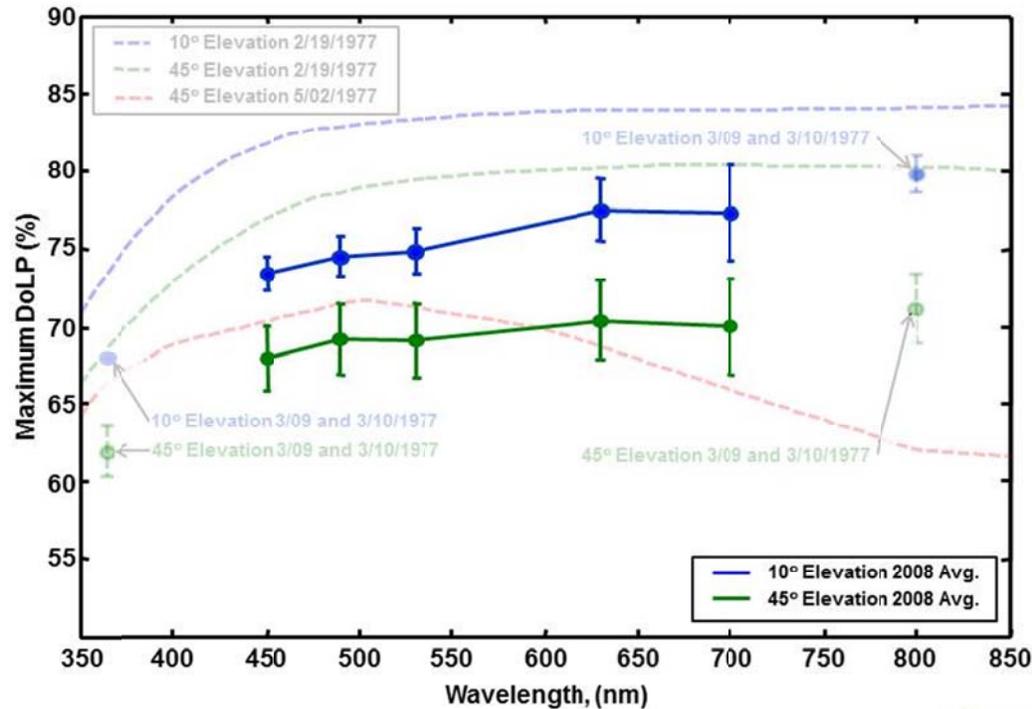

Figure 10: Maximum clear-sky DoLP vs. wavelength measured at Mauna Loa by the API in 2008 (solid font) and by Coulson (1988) in the partial background font.

The API deployment in May-June 2008 at the Mauna Loa Observatory (MLO) produced a unique data set that illustrated the importance of local surface albedo in determining sky polarization. In this case, however, it was not actually the surface albedo that was changing, but rather the clouds located BELOW the observatory, as indicated in the photograph of Fig. 11. As the clouds increased, we observed a reduction in the maximum DoLP in the sky measurements. This is caused by additional unpolarized sunlight being reflected from the clouds and mixing with the originally strongly polarized skylight. Because the underlying cloud cover tended to be consistently a strong function of time, with more clouds in the afternoon than in the morning, this effect produced an asymmetry in plots of the maximum DoLP vs. time. An example of this is shown in Fig. 12 (the plot is made with solar zenith angle on the horizontal axis rather than time to avoid shifts in the DoLP plots caused by differing sun angles at the same times on different days).

Fig. 11. Photograph looking north from the Mauna Loa Observatory, showing
that the immediate area is covered by dark lava (Mauna Kea is in the background).
During the May-June 2008 experiment clouds tended to cluster on the western
side of the island below the observatory. This produced a natural laboratory for
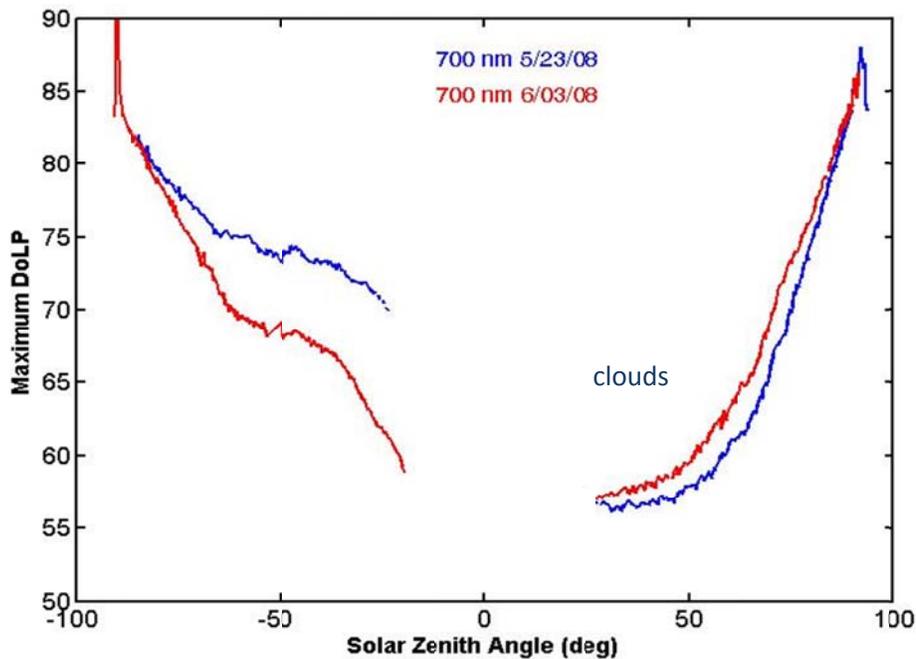studying the effect of variable surface reflectance on skylight polarization.

Fig. 12. Plot of the maximum measured DoLP vs. solar zenith angle (proportional to time) for
two full days at Mauna Loa. The blue curve (upper curve in the morning, bottom curve in the
afternoon) is from a day with few underlying clouds, while the red curve (bottom am curve, top
pm curve) is from a day with significantly more underlying clouds. (The midday gap is when the
band of maximum polarization falls below the horizon and cannot be measured).

13

Evidence of the strong surface albedo influence is provided by the difference between the morning DoLP curves on the two days shown in Fig. 11. For example, at 700 nm on 23 May (top blue line, morning data) the DoLP fell to approximately 0.72 at a zenith angle of -20˚ (east), while on 3 June (bottom red line, morning data) it fell to approximately 0.58 at the same solar angle. The sky over the observatory was clear on both days, and the 700-nm aerosol optical depth measured at the observatory remained very low (near 0.03). The major difference between these two days was that there was far less cloudiness and haze **below** the observatory on 23 May than on 3 June. This is confirmed in the satellite imagery from these two days, which are shown on the bottom of Fig. 13, along with corresponding late-afternoon all-sky polarization images (top).
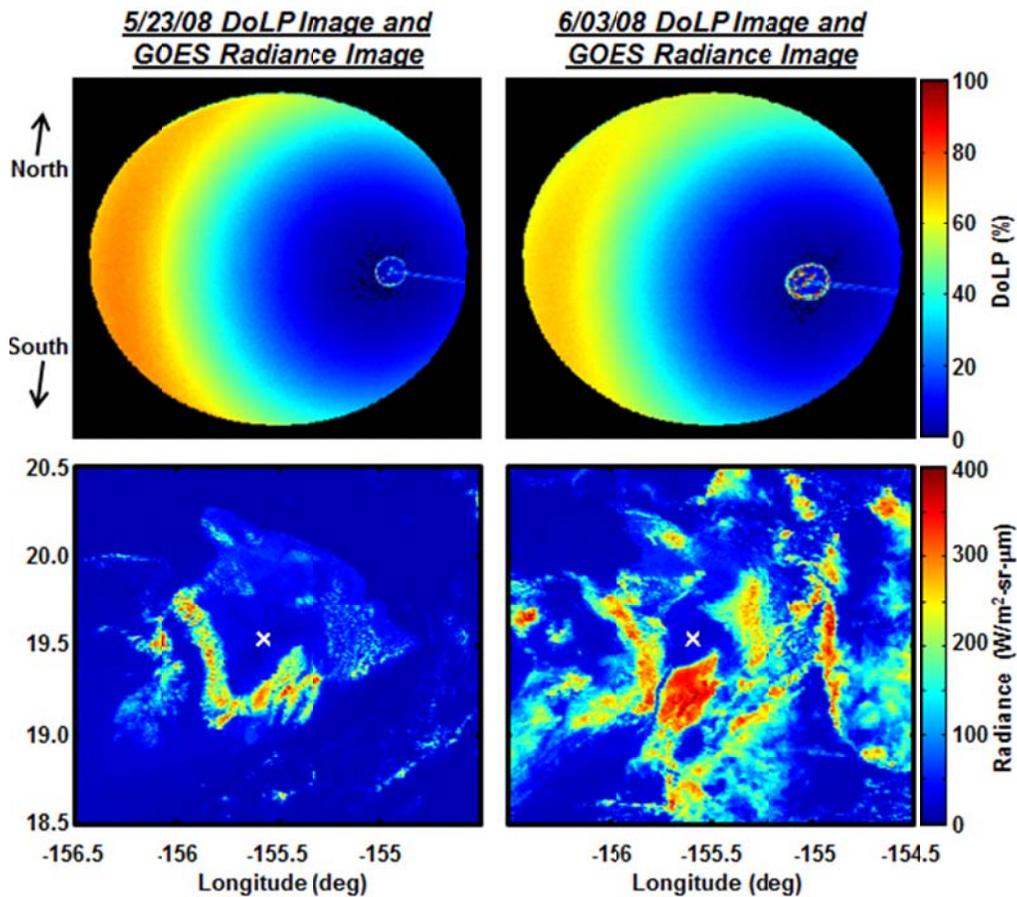

Fig. 13. Comparison of the two days from Fig. 12: (top) all-sky DoLP images, (bottom) corresponding GOES satellite images of the entire island of Hawaii. There are very clearly many more clouds around the island on 3 June relative to 23 May. Furthermore, the clouds are more uniformly clustered around the island on 3 June than on 23 May, which helps explain the stronger asymmetry for 3 June in Fig. 12

Analysis of the data from the 2008 MLO deployment allowed us to determine an initial model of the expected maximum skylight DoLP vs. upwelling radiance (which is proportional to surface albedo or reflectance). We used GOES satellite imagery, such as the images shown on the bottom of Fig. 13, to calculate the upwelling radiance for a region of 50-km radius, centered on

our instrument location (this 50-km value was determined through iterative calculations, and matches approximately the size of the island). The results are shown as plots of the max DoLP vs. upwelling radiance in Fig. 14 for the five wavelength bands of the API at that time. In all bands, the maximum skylight DoLP is reduced by a brighter underlying surface, with the strongest effect appearing at the longer wavelengths (plots of maximum skylight DoLP tend to show increased polarization at longer wavelengths because of reduced Rayleigh multiple scattering because of the 1/wavelength[4] dependence).
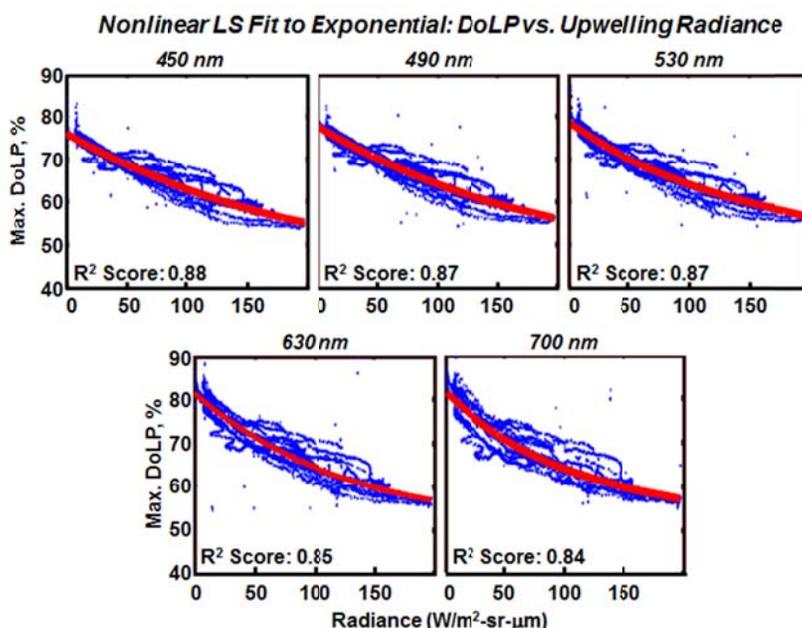

Fig. 14. Maximum DoLP vs. upwelling radiance (proportional to surface albedo or reflectance), showing that skylight becomes less polarized when the underlying surface becomes brighter.

Aerosol Measurements

Whereas the Mauna Loa deployment provided a unique opportunity to study the influence of surface brightness on skylight polarization, in fall 2009 we conducted another experiment focused on understanding the influence of variable aerosols with relatively constant surface brightness. We operated the API, our Infrared Cloud Imager (ICI), several atmospheric lidars, a sun-tracking solar radiometer, and a suite of ground-based aerosol sampling instruments loaned to us by the University of Alaska and Georgia Institute of Technology. A photograph of some of these aerosol instruments is shown in Fig. 15, including a Scanning Mobility Particle Sizer (SMPS) and Optical Particle Counter (OPC) to measure aerosol size distributions, and an integrating nephelometer to measure the aerosol scattering coefficient.

We ran these instruments together intensively through the month of September 2009 and partly into October 2009, acquiring an excellent combination of extremely clean-air conditions, punctuated with episodes of wildfire smoke. This variability is indicated by the plot of 530-nm scattering coefficient vs. time for a 24-hour period (27 Sep. 2009), obtained with the ground-based nephelometer, shown here as Fig. 15 (more polluted air has a higher scattering coefficient

because of the increased concentration of particles). Fairly intense wildfire smoke in the early morning hours gives way to quite clean air during the morning (~6:00-11:00 am), smoke increases again until about 20:00, and then shifting winds very rapidly clear the air to extremely clean valuesat and after 21:00 (Montana Daylight Savings Time). Analysis of the skylight polarization data for this aerosol experiment is still in progress and results will be included in the report for the follow-on project.
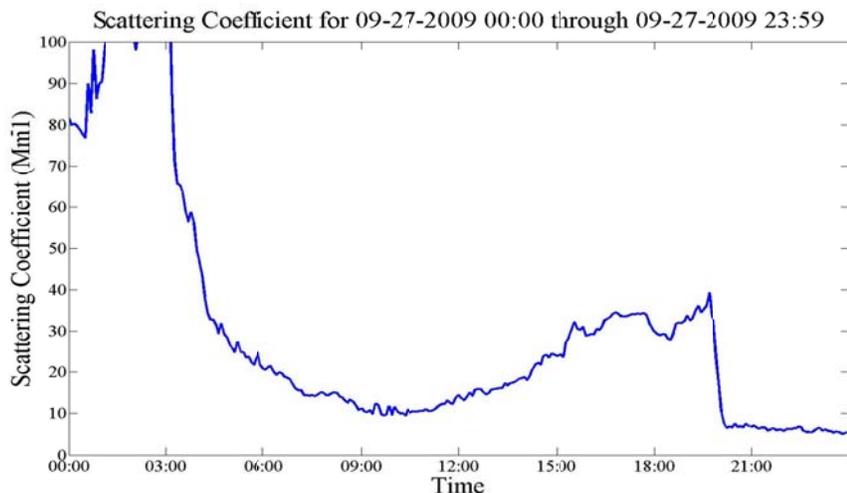

Fig. 15. Twenty-four-hour time-series plot of the scattering coefficient on 27 Sep. 2009 measured at the ground, showing the wide range of conditions obtained during the fall 2009 aerosol experiment.

References

Charlson, R. J., A. S. Ackerman, F. A.-M. Bender, T. L. Anderson, Z. Liu, "On the climate forcing consequences of the albedo continuum between cloudy and clear air," *Tellus B* **59**(4), 715-727 (2007).

Coulson, K. L., *Polarization and intensity of light in the atmosphere* (Deepak Publishing, 1988).

Cronin, T. W., E. J. Warrant, and B. Greiner, "Celestial polarization patterns during twilight," *Appl. Opt.* **45**(22), 5582-5589 (2006).

Dahlberg, A., N. J. Pust, J. A. Shaw, "All-sky polarization imaging at the Mauna Loa Observatory, Hawaii," Proc. SPIE **7461**, (*Polarization Science and Remote Sensing III,* San Diego, CA), 3-4 Aug. (2009).

Horvath, G., A. Barta, J. Gal, B. Suhai, and O. Haiman, "Ground-based full-sky imaging polarimetry of rapidly skies and its use for polarimetric cloud detection," *Appl. Opt.* **41**(3), 543-559 (2002).

Koren, I., L. A. Remer, Y. J. Kaufmann, Y. Rudich, J. V. Martins, "On the twilight zone between clouds and aerosols," *Geophys. Res. Lett.* **34**, L08805, doi:10.1029/2007GL029253 (2007).

Koren, I., L. Oreopoulous, G. Feingold, L. A. Remer, A. Altaratz, "How small is a small cloud?" *Atmos. Chem. Phys. Discuss.* **8**, 6379-6407 (2008).

Liu, Y. and K. Voss, "Polarized radiance distribution measurements of skylight. II. Experiment and data," *Appl. Opt*. **36**(33), 8753-8764 (1997).

North, J. and M. Duggin, "Stokes vector imaging of the polarized sky-dome," *Appl. Opt*. **36**(3), 723-730 (1997).

Pomozi, I., G. Horvath, R. Wehner, "How the clear-sky angle of polarization pattern continues underneath clouds: full-sky measurements and implications for animal orientation," J. Experimental Biology **204**, 2933-2942 (2001).

Pust, N. J. and J. A. Shaw, "Dual-field imaging polarimeter using liquid crystal variable retarders," *Appl. Opt.* **45**(22), 5470-5478 (2006).

Pust, N. J. and J. A. Shaw, "Digital all-sky polarization imaging of partly cloudy skies," Appl. Opt. **47**(34), H190-H198, doi:10.1364/AO.47.00H190 (2008).

Pust, N. J., J. A. Shaw, and A. R. Dahlberg, "Visible-NIR imaging polarimetry of metal surfaces viewed under a variable atmosphere," Proc. SPIE **6972** (*Polarization: Measurement, Analysis, and Remote Sensing VIII,* Orlando, FL), 18-19 Mar. (2008).

Pust, N. J., A. Dahlberg, J. A. Shaw, "How good is a single-scattering atmospheric polarization model?," Proc. SPIE **7461**, (*Polarization Science and Remote Sensing III,* San Diego, CA), 3-4 Aug. (2009a).

Pust, N. J., A. Dahlberg, J. A. Shaw, "Simultaneous measurements of polarization from metal plates and the sky," Proc. SPIE **7461**, (*Polarization Science and Remote Sensing III,* San Diego, CA), 3-4 Aug. (2009b).

Sabatke, D. S., M. R. Descour, E. L. Dereniak, "Optimization of retardance for a complete Stokes polarimeter," Optics Letters **25**, 802-804 (2000).

Shaw, J. A., N. J. Pust, B. Staal, J. Johnson, A. Dahlberg, "Continuous outdoor operation of an all-sky polarization imager," Proc. SPIE **7672** (*Polarization: Measurement, Analysis, and Remote Sensing IX*), 76720A-1-7, 7 April 2010 (doi:10.1117/12.851374).

Tyo, J. S., "Noise equalization in Stokes parameter images obtained by use of variable retardance polarimeters," Optics Letters **25**, 1198-2000 (2000).

Tyo, J. S., "Design of optimal polarimeters: maximum of signal-to-noise ratio and minimization of systematic error," Appl. Opt. **41**, 619-630 (2002).

Voss, K. and Y. Liu, "Polarized radiance distribution measurements of skylight. I. system description and characterization," *Appl. Opt*. **36**(24), 6083-6094 (1997).